More Experiment and Evaluation Details for Frequency-Guided Network for Low-contrast Dental Plaque Segmentation Beyond Human Vision

We provide more method details complementary to the paper's Experiment and Evaluation parts.

I. Parameter analysis

We analyze the critical parameters of high-frequency augmentation and the attention mechanism positions.

The high-frequency augmentation parameters. The high-frequency augmentation parameters affect the LF phase's input, influencing our methods' performance. The two main parameters are S_d and S_o. To investigate the impact of these parameters, we perform high-frequency augmentation with three different sets of parameter values on the teeth mask. This results in three datasets, namely ENHAN-1, ENHAN-2, and ENHAN-3. Then, we evaluate our methods on each dataset as the input of the LF phase to assess the mIoU and mAcc. The result are shown in Table I, We observe that the ENHAN-1 dataset performs slightly better than the other two. As a result, we empirically select the parameter values from ENHAN-1 for our methods.

TABLE I
PERFORMANCE COMPARISON OF THREE STRUCTURING ELEMENT SIZES.

Datasets	S_o	S_d	Methods	mIoU[%]	mAcc[%]
ENHAN-1	30×30	1×1	Ours-H	*73.30*	*83.75*
			Ours	**74.02**	**84.04**
ENHAN-2	30×30	3×3	Ours-H	73.22	83.35
			Ours	73.77	83.78
ENHAN-3	15×15	3×3	Ours-H	73.19	83.31
			Ours	73.89	83.81

TABLE II
PERFORMANCE COMPARISON OF ATTENTION MODULES IN FOUR POSITIONS.

Attention Modules Positions	Datasets	mIoU[%]	mAcc[%]
No attention module	ENHAN-1	73.48	83.33
	ENHAN-3	73.30	83.50
ASPP	ENHAN-1	73.38	83.50
	ENHAN-3	73.45	83.44
Edge part	ENHAN-1	73.87	84.02
	ENHAN-3	73.94	83.84
The last feature map	ENHAN-1	**74.02**	**84.04**
	ENHAN-3	73.89	83.81

The attention modules positions. Furthermore, we investigate the impact of adding the attention modules at different positions in our method. We add the channel and spatial attention modules after certain positions in parallel. Specifically, we consider four different positions for adding the attention modules: no attention module, after the ASPP module, after the edge part of the decoupling module, and after the last feature map before the final upsampling. The effect of the attention modules varies for the two variants of our method. Table II shows the results obtained for the four different positions on datasets ENHAN-1 and ENHAN-3. The results are similar for each position on both datasets, but the gaps between different positions are significant. Adding the attention modules after the last feature map results in the best performance, increasing 0.54% in mIoU and 0.69% in mAcc. Fig. 1 provides visualization results of the final layer's Gradient-weighted Class Activation Mappings (CAM). Notably, adding the attention modules after the last feature map allows the network to focus more on the areas of the teeth not covered by plaque. Although some CAM diagrams exhibit the checkerboard pattern due to grad-CAM's limitations, it does not affect the maps' interpretation.

II. Visual analysis and visualization results

Visualization results of the training process metrics. In every training phase, the training loss drops, and the validation mIoU rises with increased epochs. The training loss and validation mIoU of the HF phase are shown in Fig. 2(a). The training loss and validation mIoU of the LF phase of our methods are shown in Fig. 2(b) and Fig. 2(c). In three figures, the blue line shows mIoU, and the red line shows training loss. The left horizontal axis represents validation mIoU, the right horizontal axis represents training loss, and the vertical axis denotes epochs. The loss curve is smoothed using a smoothing rate of 0.99, while the mIoU curve is smoothed with a smoothing rate of 0.9. From these figures, it can be observed that the training loss drops, and the validation mIoU rises with the increase in epochs from 20 to 160. Although the curve of training loss shows large fluctuations after 100 epochs, it is important to note that the loss curve actually drops significantly more from 0 to 20 epochs when compared to the fluctuations seen after 100 epochs. In summary, the curves in

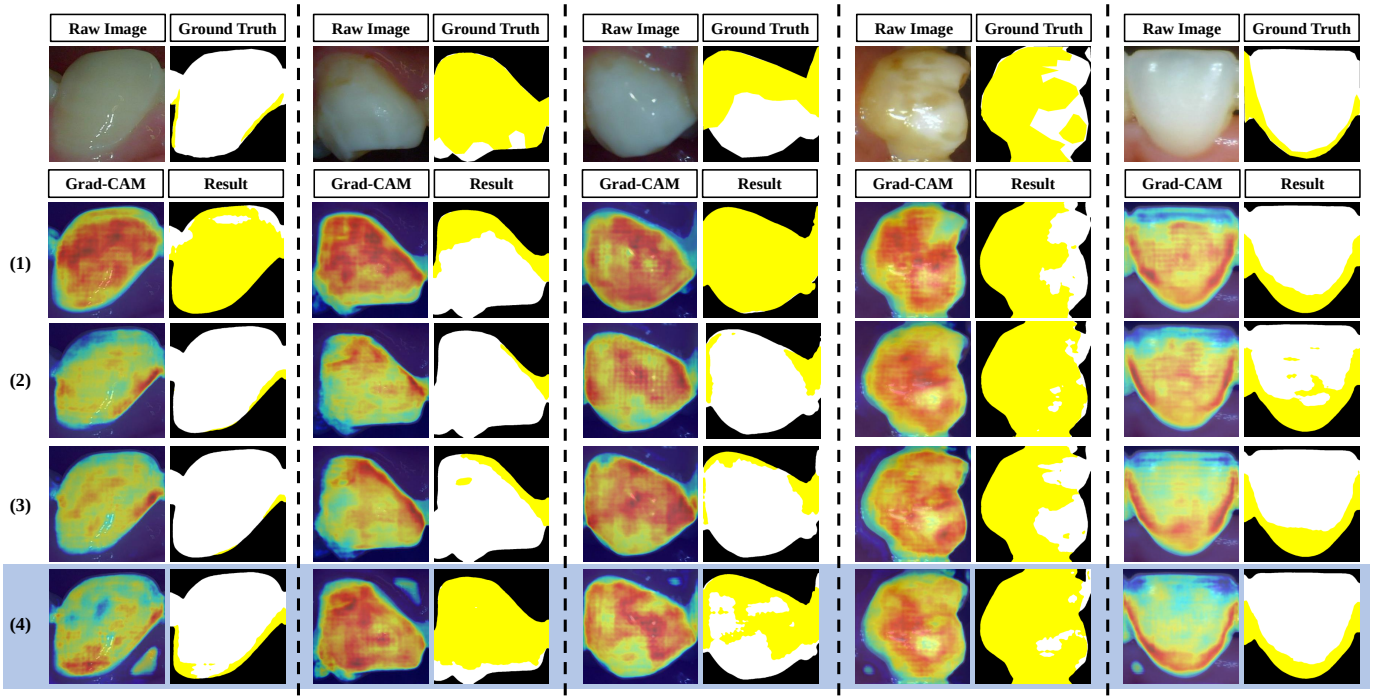

Fig. 1. Qualitative comparisons with four attention modules positions. In the top row, we demonstrate the raw image and ground truth for reference. We conduct experiments with four different positions for adding the attention modules. In the second to fifth rows, we show the results and Gradient-weighted Class Activation Mappings [1] of the final layer. Although some CAM diagrams exhibit the checkerboard pattern due to grad-CAM's limitations, it does not affect the maps' interpretation. The four positions for the attention modules are as follows: (1) no attention module, (2) attention modules added after the ASPP module, (3) attention modules added after the edge part of the decoupling module, and (4) attention modules added after the last feature map and before the final upsampling.

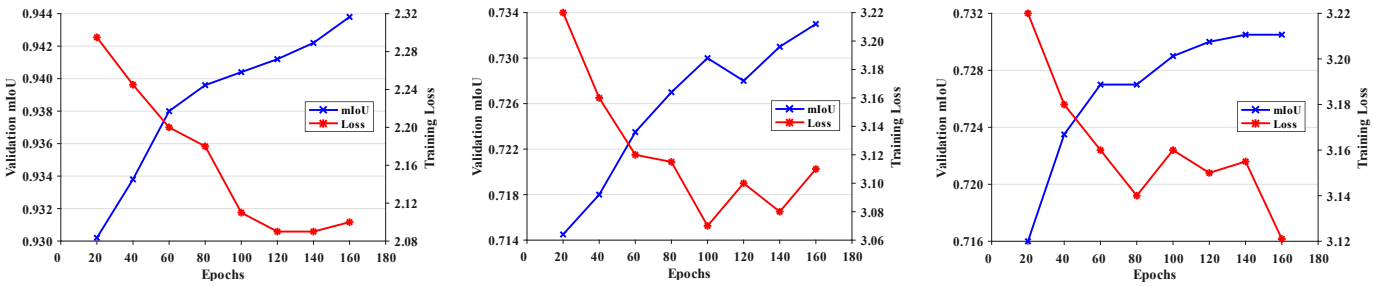

(a) Loss and mIoU of the HF phase. (b) Loss and mIoU of the LF phase of Ours. (c) Loss and mIoU of the LF phase of Ours-H.

Fig. 2. Training loss and validation mIoU of the HF and LF phases in training. (a) Shows loss and mIoU of the HF phase, (b) shows loss and mIoU of the LF phase of Ours, and (c) shows loss and mIoU of the LF phase of Ours-H.

all three figures start to fluctuate after 100 epochs, indicating that the model has been trained to its optimal performance.

Visualization results of the body and edge binary map. The visualization of the body and edge binary map generated by the HF and LF phases are shown in Fig. 3. In the HF phase, our methods focus on segmenting the teeth and non-teeth regions, resulting in a binary edge map that accurately identifies the edges of teeth. Our approaches can precisely locate the edge of teeth when some of the boundaries between teeth and gingiva are blurry. In the LF phase, we segment the plaque and non-plaque regions, leading to a binary edge map highlighting the edges of both plaque and teeth. The binary body map is complementary to the corresponding edge binary map, providing additional information on the location of plaque and teeth within the image.

REFERENCES

[1] R. R. Selvaraju, M. Cogswell, A. Das, R. Vedantam, D. Parikh, and D. Batra, "Grad-cam: Visual explanations from deep networks via gradient-based localization," in *ICCV*, 2017, pp. 618–626.

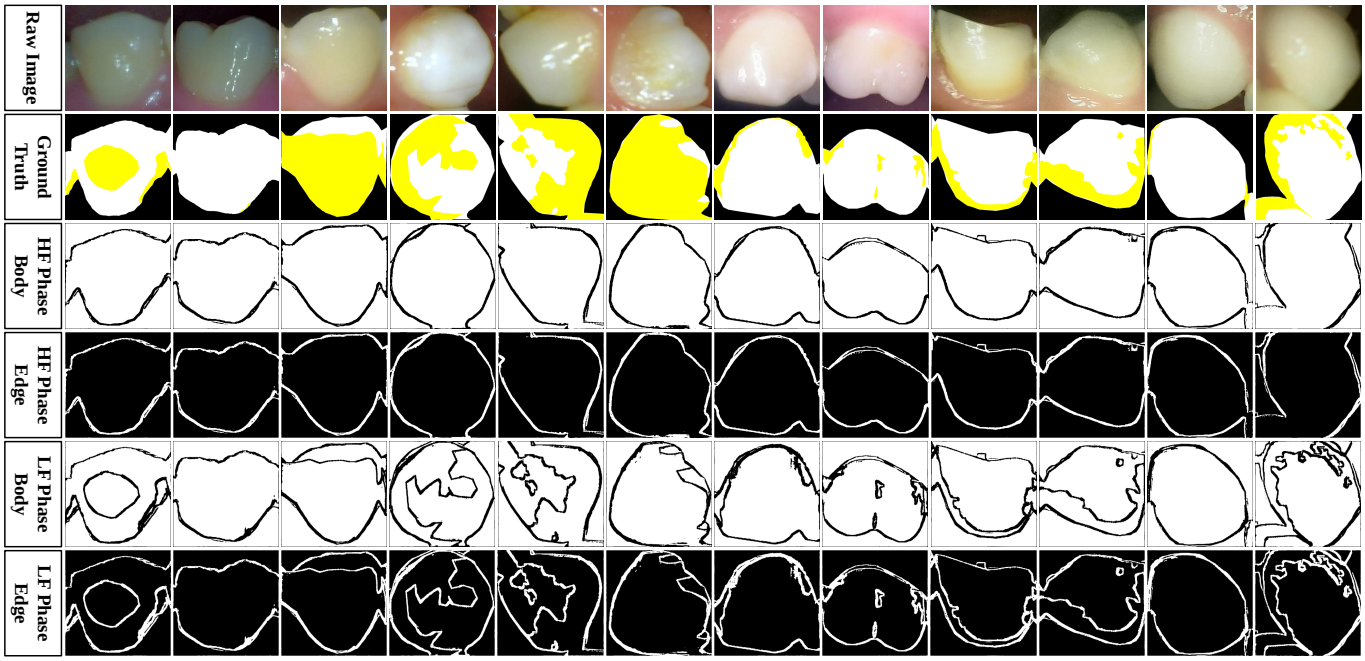

Fig. 3. Visualization segmentation results in HF and LF phases for the edge and body. The binary edge maps correspond with the boundary of teeth and plaque precisely. The binary body and edge maps are complementary to each other. The third and fourth rows of the visualization show the binary body map and the binary edge map in the HF phase, while the fifth and sixth rows show the binary body map and the binary edge map in the LF phase.